

See discussions, stats, and author profiles for this publication at: <https://www.researchgate.net/publication/283616493>

Adsorption and Deposition of Li₂O₂ on the Pristine and Oxidized TiC Surface by First-principles Calculation

ARTICLE *in* THE JOURNAL OF PHYSICAL CHEMISTRY C · OCTOBER 2015

Impact Factor: 4.77 · DOI: 10.1021/acs.jpcc.5b06492

READS

8

4 AUTHORS, INCLUDING:



Zhenyu Wang

Xi'an Jiaotong University

5 PUBLICATIONS 4 CITATIONS

[SEE PROFILE](#)



Xin Chen

Xi'an Jiaotong University

11 PUBLICATIONS 126 CITATIONS

[SEE PROFILE](#)



Chunming Niu

Xi'an Jiaotong University

49 PUBLICATIONS 2,464 CITATIONS

[SEE PROFILE](#)

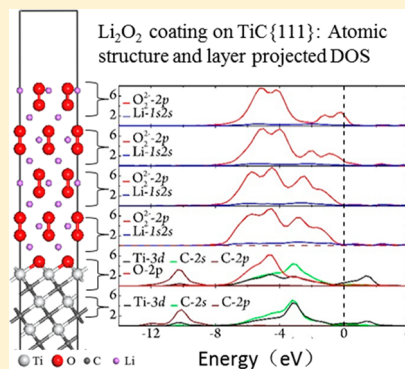
Adsorption and Deposition of Li_2O_2 on the Pristine and Oxidized TiC Surface by First-principles Calculation

Zhenyu Wang, Xin Chen, Yonghong Cheng, and Chunming Niu*

Center of Nanomaterials for Renewable Energy, State Key Lab of Electrical Insulation and Power Equipment, School of Electrical Engineering, Xi'an Jiaotong University, 99 Yanxiang Road, Xian 710054, China

S Supporting Information

ABSTRACT: We investigate Li_2O_2 adsorption and deposition on the low index surfaces of pristine and oxidized TiC, which has been demonstrated recently to be an excellent cathode for Li–air batteries. We found that the pristine TiC surface is not stable toward interaction with Li_2O_2 and that surface stability can be enhanced greatly by surface oxidation as shown by surface energy reduction from 102 to 23 meV/ \AA^2 for the TiC{100} surface and from 208 to 39 meV/ \AA^2 for the TiC{111} surface after oxidation. Adsorption of two Li_2O_2 clusters on the 2×2 Ti-terminated TiC{111} surface (TiC{111}–Ti) resulted in spontaneous destruction of Li_2O_2 clusters and formation of a saturated periodic two atomic layer coating in which each O atom is bonded to three Ti atoms to form an O layer equivalent to the layer formed by O_2 surface oxidation, and Li atoms sit on the top. The atomic arrangement of O and Li layers resembles that of Li_1O_2 layers normal to the [0001] direction in the Li_2O_2 crystal structure. Interface models constructed based on this lead showed that the growth of Li_2O_2 can be continued on oxidized TiC{111}–Ti through a surface conduction mechanism to form Li_2O_2 coating with lattice parameters almost identical to those of the standard Li_2O_2 unit cell. On the oxidized TiC{100} surface (TiC{100}– TiO), two Li_2O_2 clusters adsorbed on two adjacent Ti sites by Ti–O bonding with the O–O axis in Li_2O_2 perpendicular to the surface resulted in a Li and O atom configuration which is similar to $\text{O}_2\text{Li}_3\text{O}_4$ layers in the Li_2O_2 crystal structure, indicating a potential path for Li_2O_2 nucleation on the TiC{100}– TiO surface. Interface models by following this path suggested that Li_2O_2 coating may be grown on the TiC{100}– TiO surface with a dihedral angle between 11.4° and 22.4°, and strains inside the Li_2O_2 could induce conductivity. These atomistic insights are in good agreement with the experimental findings.



1. INTRODUCTION

The Li–air (O_2) batteries first reported by Abraham and Jiang¹ are continuously attracting great attention because of their high specific theoretical energy with potential to meet the demands of applications requiring high energy density, such as the power source for the next generation of electric vehicles. The chemistry of Li–air batteries is simple, relying on the electrochemical reaction between metallic Li and O_2 from the air, which generates two potential products, Li_2O_2 and Li_2O . Both are insulators. It has been demonstrated that Li_2O_2 is electrochemically reversible and Li_2O is not.^{2,3} There is still some uncertainty regarding whether Li_2O is a discharging product or from side reactions.⁴ To date, the cathode remains to be a major challenge to demonstrate the feasibility of Li–air batteries. The cathode needs to be conductive for electron transport, porous to accommodate the discharge product Li_2O_2 , and stable but with sufficient active surface sites to facilitate effective formation and decomposition of Li_2O_2 during charge and discharge cycles. The efficiency of this cycle of the reactions is determined largely by the thermodynamics and kinetics of cathodic oxygen reduction and evolution involving highly reactive oxygen species. The major barriers, such as high electrode overpotential (4.0–4.5 V during charge)^{2,5–10} which

leads to low round trip efficiency, limited capacity retention and cycle life,^{2,4–6,8,11–15} and poor electrochemical stability of both electrode and electrolyte,^{14–17} remain to be overcome. From the beginning, the porous carbon was the choice of the cathode. However, carbon is not stable^{17–21} above 4 V versus Li/Li⁺. It has been found that carbon not only decomposes itself during charging but also catalyzes decomposition of aprotic electrolytes resulting in the formation of Li₂CO₃ which deposits on the surface of the cathode leading to capacity fading and cell death. There are some successes in reduction of overpotential by using MnO₂, Au, and Pt as catalysts^{2,5–10,22,23} in the cathode. Bruce's group showed that the nanoporous gold cathode combined with an electrolyte based on dimethyl sulfoxide (DMSO) exhibits very good stability.¹¹ Unfortunately, the high mass density of the gold cathode reduces specific energy density which takes away the key advantage of high specific energy offered by Li–air cells over Li ions. Furthermore, gold is too expensive to be commercially viable. Recently, the same group reported¹⁸ that a cathode based on

Received: July 7, 2015

Revised: October 14, 2015

TiC can overcome the disadvantages of carbon and nanoporous gold. It greatly reduces side reactions at the electrolyte–cathode interface compared with carbon, is more stable than nanoporous gold, and delivers more than 99.5% purity of Li_2O_2 formation on each discharge and its complete oxidation on charge, with over 98% capacity retention after 100 cycles. They attributed this excellent performance to the electric conductivity of TiC and the formation of oxide layers on the TiC surface.

Bulk TiC, TiC surface, adsorption on the TiC surface, as well as the interface of TiC^{24–27} with transition metals have been subjected to extensive theoretical study.^{28,29} Because of its role in Li–air batteries, Li_2O_2 has attracted a great deal of theoretical attention lately. Radin et al.³⁰ predicted the bulk Li_2O_2 is an insulator with a band gap from 5.15 to 6.37 eV. Viswanathan et al.³¹ built theoretical models which suggested that conduction relied on electron tunneling can only support 5–10 nm thick insulating Li_2O_2 formation. However, this could not explain 100 cycles of capacity retention with the observed Li_2O_2 crystallite size of several hundred nanometers.¹³ In practice, crystallites are rarely perfect. The surface states, defects, dislocations, and impurities all could result in conduction pathways. Indeed, Hummelshøj et al.³² showed that lithium vacancies induce conductivity in bulk Li_2O_2 . Geng et al.³³ showed that certain grain boundary could induce conductivity in Li_2O_2 . Radin et al.³⁴ carried out DFT calculations of 40 different surfaces of Li_2O_2 and Li_2O . They identified several oxygen-rich {0001} and {1100} surface terminations that are stable and half-metallic. On the contrary, the most stable surfaces for Li_2O are stoichiometric and insulating. The difference in surface electronic properties may explain observations of electrochemical reversibility of Li_2O_2 because of surface electron paths despite that its bulk is insulating, and irreversibility of Li_2O for it lacks electron pathways.

In a previous letter,³⁵ we reported the preliminary result of Li_2O_2 cluster adsorption and deposition on the TiC{111} surface. In this paper, we provide a full account of the study of Li_2O_2 cluster adsorption and deposition on low index surfaces of TiC as well as effects of surface oxidation of TiC on both processes. The bulk properties of TiC and Li_2O_2 were calculated and compared with those reported in the literature to test the accuracy of our approximation. Geometric structure and surface energies of selected low index surfaces of both TiC and Li_2O_2 were calculated to aid the selection of surfaces for the construction of interface models. Surface oxidation was approximated by replacing C atoms in the top layer of the supercell for the TiC{100} surface and by formation of a periodic O layer through O_2 adsorption on the top of Ti for the Ti-terminated TiC{111} surface. Li_2O_2 cluster adsorption on both pristine and oxidized TiC surfaces was studied to establish chemical bonding and gain insight into nucleation initiation of Li_2O_2 deposition on the TiC surface. Finally, interface models were built, and structural and electronic properties of interface and Li_2O_2 coating were investigated.

2. COMPUTATIONAL DETAILS AND SURFACE CONFIGURATION

All calculations in this work were carried out by first-principles calculation based on the periodic density functional theory (DFT), as implemented in CASTEP code,^{36,37} in which the interactions between the ions and valence electrons were described by Vanderbilt ultrasoft pseudopotentials³⁸ using the

generalized gradient approximation (GGA).³⁹ The atomic configurations of Ti, C, O, and Li generated from the ultrasoft pseudopotential were $3s^23p^63d^24s^2$, $2s^22p^2$, $2s^22p^4$, and $1s^22s^1$, respectively.

The Broyden–Fletcher–Goldfarb–Shannon (BFGS)⁴⁰ algorithm was adopted to minimize the total energy of the models and seek the ground state. For geometry optimization, the final convergent values were set at 2.0×10^{-5} eV/atom for total energy, 0.05 eV/Å for force, 0.1 GPa for maximum stress, 1.0×10^{-5} eV/atom for band energy, and 0.002 Å for the maximum displacement. A kinetic energy cutoff value was set to 385 eV for all calculations involving TiC, and a cutoff energy of the plane-wave basis was set to 405 eV for all calculations of pure Li_2O_2 .

The k-point meshes were set at $11 \times 11 \times 11$ for the TiC bulk unit cell and $11 \times 11 \times 1$ for its surface slabs using the Monkhorst–Pack scheme,⁴¹ and a vacuum thickness of 12 Å was employed on both sides of the surface to ensure vanishing wave function overlap across the vacuum region. The k-point mesh was set at $7 \times 7 \times 7$ for the Li_2O_2 bulk unit cell and $7 \times 7 \times 1$ for its surface slabs, including a 10 Å vacuum region on both sides. For Li_2O_2 cluster adsorption, $2 \times 2 \times 1$ TiC surface slabs including a 9 Å vacuum region were used, and the k-point mesh was set to $3 \times 3 \times 1$. Note that the same mesh size was used by Zhang et al.⁴² when O_2 adsorption on the TiC surface was studied. The interface slabs were created by joining the surface of Li_2O_2 coating with the substrate TiC. The 2×1 $\text{Li}_2\text{O}_2\{1\bar{1}00\}/\text{TiC}\{110\}$ supercell and 2×2 $\text{Li}_2\text{O}_2\{0001\}/\text{TiC}\{111\}$ supercells were constructed to study Li_2O_2 deposition on the TiC{110} and TiC{111} surface, respectively, and both employed a 10 Å vacuum region and a $5 \times 5 \times 1$ k-point mesh. For deposition on the TiC{100} surface, a 2×2 $\text{Li}_2\text{O}_2\{0001\}/\text{TiC}\{100\}$ supercell with the same thickness of the 10 Å vacuum region was used, and the k-point mesh was set at $3 \times 3 \times 1$ to reduce calculation time because of a larger number of the atoms involved.

The surface energies (γ) were calculated using the following equation

$$\gamma = \frac{1}{2A}(E_{\text{slab}} - N_A\mu_A - N_B\mu_B) \quad (1a)$$

which was first proposed by Fiorentini et al.,⁴³ where E_{slab} is the total energy of the slab and E_{bulk} is the total energy of bulk. N_A and N_B are the number of the atom A and the atom B in the slab, and μ_A and μ_B correspond to their chemical potential. In $N = N_{\text{slab}}/N_{\text{bulk}}$, N_{slab} and N_{bulk} represent the number of formula units in the slab and bulk, respectively. The fraction of 1/2 accounts for the two surfaces of the slab. The A stands for the surface area. If the slab is stoichiometric, the equation above can be written as

$$\gamma = \frac{1}{2A}(E_{\text{slab}} - NE_{\text{bulk}}) \quad (1b)$$

The adsorption energies (E_{ad}) were calculated using the following formula

$$E_{\text{ad}} = E_{\text{sub-ad}} - E_{\text{sub}} - E_{\text{mol}} \quad (2)$$

where $E_{\text{sub-ad}}$ and E_{sub} are the total energy of the adsorption system and substrate slab. E_{mol} represents the total energy of adsorbed molecules.

The geometrical aspect of matching Li_2O_2 to the TiC substrate was evaluated by calculating a misfit factor η as

defined in eq 3. We assumed that the surface of the TiC substrate remains unchanged.

$$\eta = \left| 1 - \frac{2\Omega}{\Omega + A} \right| \times 100\% \quad (3)$$

where Ω is the surface area of the TiC substrate, and the A stands for the surface area of the covering Li_2O_2 surface cell.

The Mulliken population analysis was used to reveal the nature of the chemical bonds at the interface. The average bond length \bar{L} and the average overlap bond population \bar{n} were defined as follows

$$\bar{L}(A - B) = \frac{\sum L_i N_i}{\sum N_i} \quad (4a)$$

$$\bar{n}(A - B) = \frac{\sum n_i N_i}{\sum N_i} \quad (4b)$$

$$N_i = \sum_j n(A_i - B_j) \quad (4c)$$

where L_i and n_i are the bond length and overlap bond population between atom A_i and atom B_j , respectively. N_i is the total overlap bond population between A_i and B_j .

The ideal work of adhesion W_{ad} is a rough approximation of the energy required to separate the coating from the substrate at the interface, which is defined as

$$W_{ad} = \frac{\sum_i E_i - E_{\text{TiC}/\text{Li}_2\text{O}_2}}{\Omega} \quad (5)$$

where E_i is the total energy of slab i ($i = \text{TiC}, \text{Li}_2\text{O}_2$); $E_{\text{TiC}/\text{Li}_2\text{O}_2}$ is the total energy of the interface system; and Ω is the interface area.

3. RESULTS AND DISCUSSION

3.1. Bulk and Surface Properties of TiC and Li_2O_2 . TiC has a rock salt NaCl structure (Figure S1a in Supporting Information), in which two fcc sublattices formed independently by Ti and C atoms interlace together by a shift of [1/2, 1/2, 1/2]. A hexagonal crystal structure (Figure S1b in Supporting Information) of Li_2O_2 generally accepted now was reported by Föpple in 1957,⁴⁴ in which the arrangement of oxygen and Li ions can be described as repeated planes of AcBcAbCbA,⁴⁵ where capital letters refer to lithium and small letters to oxygen which is presented in O–O pairs with a bond length of 1.56 Å. For TiC, we calculated an equilibrium lattice value of 4.333 Å and a formation energy of 1.920 eV/atom, very close to the experimental values of 4.313–4.330 Å^{46–48} and −1.897 eV,⁴⁹ respectively, and also calculated DFT values of 4.348 Å and −1.91 eV by Arya et al.²⁷ For Li_2O_2 , our calculated equilibrium lattice values are $a = 3.178$ Å and $c = 7.751$ Å, both slightly larger than the corresponding experimental values⁴⁵ and comparable to calculated DFT values from several groups,^{34,50,51} and the formation energy is −6.01 eV, very close to both the experimental (−5.929 eV)⁴⁹ and DFT value (−5.99 eV).³⁴ In our calculation, a correction to well-known oxygen over bonding problem was applied to the Li_2O_2 calculation using a method reported by Hummelshøj et al.³²

The surface energies of low-index TiC surfaces were approximated using eqs 1a and 1b of the slab models. The results from {100} and {110} surfaces together with those³⁵ from {111} are summarized in Table 1. For comparison, the

Table 1. Surface Energy of TiC Low Index Surface and Oxidized TiC{100} and {111} Surfaces

surface	termination	γ (meV/Å ²)	
		this work	ref 27
{100}	TiC	102	104
	TiO	23	-
{110}	-	226	227
	Ti	208 ^a	195
{111}	C	504	-
	O	39 ^a	-

^aThese data are reproduced from our previous letter.³⁵

surface energies of the corresponding surfaces reported by Arya et al.²⁷ are also listed in the table. It can be seen that our results are in agreement with Arya et al. The TiC{100} surface is the most stable, with a surface energy well below those of {111} and {110}. There are two possible terminations for the {111} surface, one with Ti (TiC{111}_Ti) and the other with C (TiC{111}_C). The TiC{111}_Ti surface is much more stable than the TiC{111}_C surface. The stability of the TiC{110} surface is poorer than TiC{111}_Ti but much higher than TiC{111}_C. Attempt of Wulff construction for TiC resulted in a cube terminated by {100} equivalent surfaces (Figure S1A in Supporting Information), which suggests a TiC{100} surface domination in TiC crystallites at thermal dynamic equilibrium.

It has been known that the TiC surface is not stable toward oxidation. Shirotori et al.⁵² investigated the TiC{100} surface by XPS and LEED and found that when the surface is exposed to O_2 at room temperature the C atoms on the surface of the substrate are depleted and the Ti atoms are oxidized to form a disordered TiO_x (1.5 < x < 2.0) layer. Ottakam et al.¹⁸ found that the surface of their as-received TiC contained significant proportions of TiO_2 and TiOC . The proportion of TiO_2 increased further upon the first discharge and remained the same thereafter. They attributed TiC electrode stability to this surface oxidation. We approximate the surface oxidation by replacing C atoms with O atoms in the top layer of the TiC{100} surface and carried out DFT calculation. Interestingly, the replacement of surface C atoms with O atoms greatly reduced the surface energy of TiC{100} from 102 to 23 eV/Å² (Table 2), which suggests a substantial improvement of the surface stability. For oxidation of the TiC{111}_Ti surface, as

Table 2. Surface Energy of the Li_2O_2 Low Index Surface with Different Terminations^a

surface	termination ^b	surface energy (meV/Å ²)			
		this work	ref 54	ref 55	ref 34
{0001}	$\text{Li}_1\text{O}_2\text{Li}_3\text{O}_4$	108	68		
	$\text{O}_2\text{Li}_3\text{O}_4$	6	25	41	6
	Li3	123	84		
{1̄100}	$\text{Li}_2\text{O}_2\text{Li}_3$	93	103		
	O2Li3	43	37		25
	$\text{Li}_1\text{O}_2\text{Li}_3$	18	34		34
	$\text{Li}_1\text{O}_1\text{Li}_2\text{O}_2\text{Li}_3$	32	45		31
{11̄20}	$\text{Li}_1\text{O}_1\text{Li}_3\text{Li}_2\text{O}_2\text{Li}_3$	38		52	52
	$\text{Li}_1\text{O}_1\text{Li}_2\text{O}_2\text{Li}_3$	43	43		36
	O1Li3Li2O2Li3	41		43	26

^aMore terminations are included in Table S1 in the Supporting Information. ^bLabeling scheme for surface termination is described in Figure S2 in the Supporting Information.

reported in our previous letter,³⁵ we carried out study of O₂ adsorption on the Ti-terminated TiC{111} surface and found that the TiC{111}_Ti surface is readily oxidized by interaction with O₂ molecules. Two O₂ adsorptions on the 2 × 2 TiC{111}_Ti surface resulted in the formation a periodic O layer with O atoms localized at the hcp hollows of the facial Ti atoms. The calculated average Ti–O bond length is 1.984 Å, in the range of Ti–O bond length of 1.91–2.04 Å in TiO₂.³³ A surface energy of 39 eV/Å² was calculated for this oxidized TiC{111}_Ti surface. Similar to the TiC{100} surface, surface oxidation leads to substantial surface energy reduction, increasing surface stability.

Figure 1 compares angular momentum projected local density of states (LDOS) of the top atomic layer, subatomic

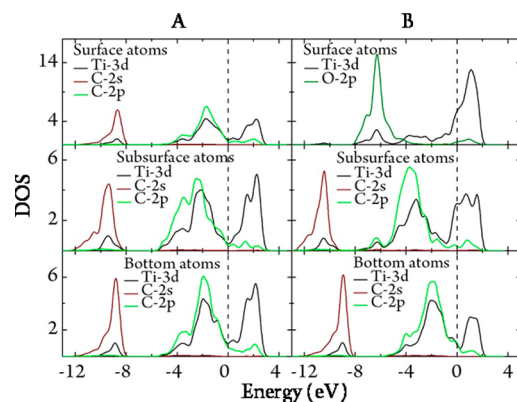


Figure 1. Comparison of angular momentum projected LDOS of the (A) pristine TiC{100} surface and the (B) oxidized TiC{100}_TiO₂ surface.

layer, and bottom atomic layer of the slab model of the pristine and oxidized TiC{100} surface. It can be seen that surface oxidation has led to a significant change of the distribution of LDOS. The conduction band edge shifted downward ~0.7 eV. Although the DOS at the Fermi level for the bottom layer did not change much, the DOS at the Fermi level for both the top and subsurface layer increased greatly, indicating a strong surface conductivity enhancement. More importantly, the hybridization of the Ti-3d orbital with O-2p opened up a pseudogap of ~5 eV, compared to the gap of ~2 eV for the hybridization between Ti-3d and C-2p of the pristine TiC surface, which explains why surface oxidation reduced the surface energy from 102 to 23 eV/Å².

Surface energies of three low index surfaces of Li₂O₂{0001}, Li₂O₂{1̄100}, and Li₂O₂{11̄20} with various terminations were evaluated. Selected terminations with relatively low energies are summarized in Table 2. For comparison, results from three publications^{34,54,55} are also listed. For all three directions, the most stable surface terminations are all oxygen rich. The O₂Li₃O₄ is the most stable termination for the {0001} surface (58.3% of Wulff shape surface, Figure S1B in Supporting Information), which is in agreement with Radin et al's calculation,³⁴ and the most stable surfaces for {1̄100} (41.7% of Wulff shape surface, Figure S1B in Supporting Information) and {11̄20} are the Li₁O₂Li₃ and Li₁O₁Li₃Li₂O₂Li₃, respectively.

We have also investigated the electronic properties of the stable surface of Li₂O₂. In agreement with Radin et al's calculation,³⁴ for the Li₂O₂{0001}_O₂Li₃O₄ surface, the spin up and spin down band structure is asymmetric (Figure S3 in

Supporting Information); the spin up states are insulating; while the spin down states are conductive induced by two partially depleted valence-band-derived spin down surface states that cross the Fermi level, indicating that the Li₂O₂{0001}_O₂Li₃O₄ surface is indeed half-metallic.

3.2. Adsorption of Li₂O₂ Clusters on the TiC Surface.

All calculations of adsorption were carried out using slab models with a 2 × 2 surface unit cell, and a thickness of four layers was used for the TiC{111} surface and five layers for TiC{100}. Li₂O₂ clusters were placed on top of the slab in various configurations and then relaxed to their equilibrium position. During the relaxation, we kept the atoms in the bottom two layers of the slab in their bulk crystallographic position. The atom positions in the rest of the layers of the slab were allowed to change together with Li and O atoms from the Li₂O₂ clusters. A planar Li₂O₂ structure (Figure S1c in Supporting Information), a rhombus parallelogram with two Li and two O atoms at four corners facing themselves diagonally, was used as the initial Li₂O₂ configuration. This configuration was first reported by Lau et al.³⁶ The O–O length in the Li₂O₂ cluster is 1.56 Å. Note that O atoms in Li₂O₂ crystals (Figure S1b in Supporting Information) are also paired^{44,45} with a slightly shorter distance of 1.55 Å between two O atoms.

Adsorption on TiC{111}. As discussed above, there are two types of atomic terminations for the TiC{111} surface, TiC{111}_C and TiC{111}_Ti. The surface energy of the TiC{111}_C termination is much higher than that of TiC{111}_Ti termination (Table 1). Our attempt to adsorb Li₂O₂ clusters on the TiC{111}_C surface resulted in complete destruction of the surface C layer, which is consistent with the unstable nature of the TiC{111}_C surface. Therefore, in the following section we only present results from the TiC{111}_Ti surface.

First, we considered single Li₂O₂ cluster adsorption on the TiC{111}_Ti surface. Two types of models were constructed, one with a planar Li₂O₂ cluster in parallel to the TiC{111}_Ti surface (denoted as C-Ti), which has been reported in our previous letter,³⁵ and the other with a planar Li₂O₂ cluster in perpendicular (O–O axis normal to the surface). We found that for the parallel models, no matter where the initial Li₂O₂ cluster was placed, O atoms and Li atoms would move to the hcp hollows of facial Ti atom positions and the fcc hollows of extrapolated C atom positions on the top, respectively (Figure 2A1),³⁵ resulting in destruction of the original flat rhombus parallelogram structure of Li₂O₂. It is very interesting that for the perpendicular model, when the O–O pair is lined on the top of the surface Ti atom (denoted as top-Ti model), adsorption is stable with O–O bond length shortened from 1.560 to 1.445 Å (Figure 2A2). However, when we attempted to move the same oriented Li₂O₂ cluster to a hollow site, the structure relaxed to the final atomic configuration of the single molecule parallel model (Figure 2A1), i.e., O atoms to the hcp hollows and Li to the fcc. The same happened when we tried to add another Li₂O₂ cluster to both the one molecule parallel and one molecule perpendicular models. Two Li₂O₂ cluster adsorption saturated the 2 × 2 TiC{111}_Ti surface, and O and Li atoms are self-assembled into the Li₁O₂ configuration (Figure 2A3) as the Li and O layers in the Li₂O₂ crystal structure (Figure S2 in Supporting Information), suggesting the initiation of nucleation of Li₂O₂ on the TiC{111}_Ti surface with Ti–O as interfacial bonding.³⁵

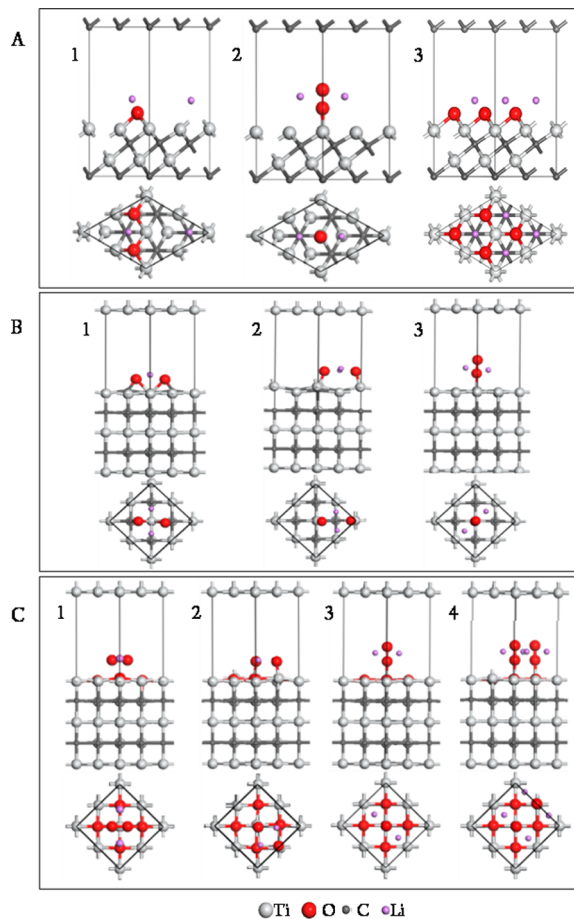


Figure 2. Side and top view of the relaxed structure of the Li_2O_2 cluster adsorbed on the TiC surface. On the $\text{TiC}\{111\}$ _Ti surface: (A1) parallel adsorption of the single Li_2O_2 cluster (C-Ti), (A2) perpendicular adsorption on the top of the Ti (Top-Ti) atom, and (A3) parallel adsorption of two Li_2O_2 clusters (C-Ti). On the $\text{TiC}\{100\}$ surface: (B1) parallel adsorption across Ti (C-Ti), (B2) parallel adsorption across C (C-C), and (B3) perpendicular adsorption on Ti (Top-Ti). On the $\text{TiC}\{100\}$ _TiO surface: (C1) parallel adsorption across Ti (C-Ti), (C2) parallel adsorption bridge of two Ti (B-Ti), (C3) perpendicular adsorption on the top of the Ti atom of one Li_2O_2 cluster, and (C4) perpendicular adsorption on the top of two Ti atoms of two Li_2O_2 clusters. A1 and A3 are reproduced from our previous letter.³⁵

The adsorption energy for the parallel model of one Li_2O_2 cluster adsorption (Figure 2A1 and C-Ti in Table 3) is -10.572 eV per Li_2O_2 cluster. When another Li_2O_2 cluster is added (Figure 2A3), the adsorption energy decreased slightly to -10.056 eV per cluster. For the perpendicular model (Top-Ti on {111} in Table 3), the adsorption energy is -3.051 eV per Li_2O_2 cluster. It is obvious that the perpendicular adsorption is less favorable energetically than the parallel adsorption. Note that the planar structure of Li_2O_2 is kept intact for the perpendicular adsorption, while it was destroyed for the parallel model. To reveal chemical bonding nature, we carried out Mulliken population analysis using eqs 4a–4c. The average bond length and overlap population for both parallel and perpendicular adsorption are listed in Table 3. As can be seen, the calculated bond populations for the Ti–O bond are all positive, suggesting attractive interaction. For the perpendicular adsorption, a stronger Ti–O bonding is evidenced by a shorter average bond length and a relatively

larger overlap population number but with a low adsorption energy because only one of the two O atoms is bonded to the surface Ti with a single Ti–O bond. For the parallel adsorption, both O atoms are bonded to the surface, and each forms three Ti–O bonds, resulting in higher adsorption energy of -10.572 eV despite the longer average Ti–O bond length. Contrary to the Ti–O bonds, the average overlap population between Ti–Li is all negative. This can be explained by the electrostatic repulsion between positive charged Li and Ti atoms, resulting from partial ionic bonding of Ti–C and Li–O bonds.

To understand electronic properties, we calculated the local density of states (LDOS) at the interface. Figure 3A shows the angular momentum projected LDOS around the interface for two parallel two Li_2O_2 cluster adsorption on the $\text{TiC}\{111\}$ _Ti surface before (substrate) and after adsorption (with Li_2O_2). It can be seen that the distribution of Ti-3d DOS changed substantially across the spectrum after adsorption. The four peaks above the Fermi level were reduced to three, and DOS at the Fermi level was reduced and spread downward to -7 eV. Between 2 and 7 eV, there is overlap between Ti-3d and O-2p states, which is consistent with the conclusion of Mulliken overlap population analysis. The DOS of O-2p is largely localized between -4 and -7 eV, and the DOS of Li-1s2s is largely distributed near and above the Fermi level, in agreement with the negative Ti–Li overlap population of Mulliken analysis.

Adsorption on the $\text{TiC}\{100\}$ Surface. Two types of surface terminations, the pristine $\text{TiC}\{100\}$ surface and TiO layer-terminated $\text{TiC}\{100\}$ surface, were studied. On the pristine $\text{TiC}\{100\}$ surface, two single Li_2O_2 cluster adsorption models were constructed for the parallel adsorption (planar Li_2O_2 molecule in parallel with the $\text{TiC}\{100\}$ surface): one with O–O in Li_2O_2 across the center Ti atom (denoted as C-Ti) in parallel with the Ti–C–Ti–C–Ti chain, while Li–Li was lined perpendicular to it (Figure 2B1), and the other with the same orientation but O–O across a C atom (denoted as C-C, Figure 2B2). After relaxation, in both cases, orientation of O–O and Li–Li lines relative to the $\text{TiC}\{100\}$ surface remained the same, but the O–O bond in the Li_2O_2 cluster was broken. The O atoms in both cases formed bonds with both Ti and C atoms, broke away from the Li atoms in the initial planar structure, and moved closer to the $\text{TiC}\{100\}$ surface. One noted that the difference between the two models is that the surface atomic structure of the relaxed Ti-cross model (Figure 2B1) remained flat, while the Ti atoms which formed a bond with O atoms in C-cross model moved away from the surface slightly. This surface instability became more profound when we tried to add another Li_2O_2 cluster to the surface. Two Li_2O_2 adsorption is stable for the Ti-cross model which led to surface destruction for the C-cross model. The adsorption energy for the Ti crossover model (C-Ti of {100} in Table 3) is -3.506 eV per Li_2O_2 for single Li_2O_2 adsorption and slightly increased to -3.696 eV for the same model with two Li_2O_2 adsorption, which is larger than the C-cross site adsorption energy, -2.316 eV per Li_2O_2 . For the perpendicular configuration, there are two feasible adsorption sites, one over the top of a Ti atom (Top-Ti) and the other over the top of a C atom (Top-C). We could not get a convergent calculation for the top-C model. We found that for the Top-Ti model (Figure 2B3) the Li_2O_2 molecule can be adsorbed, but with a much smaller adsorption energy of -0.636 eV (Top-Ti on {100} in Table 3).

Next, we directed our attention to the $\text{TiC}\{100\}$ surface terminated with a TiO layer. The structural and electronic

Table 3. Li_2O_2 Cluster Adsorption on the TiC Surface: Adsorption Energy, Average Bond Length, and Mulliken Overlap Population

surface	$n\text{Li}_2\text{O}_2$	adsorption site	bond	$L_{\max}(\text{A}-\text{B})/\text{\AA}$	$L_{\min}(\text{A}-\text{B})/\text{\AA}$	$\bar{L}/\text{\AA}$	\bar{n}	E_{ad}/eV
$\text{TiC}\{111\}_{-\text{Ti}}$	1	C-Ti ^b	Ti-O	2.236	2.229	2.234	0.35	-10.572
			Ti-Li	2.927	2.760	2.849	-0.13	
			Ti-O	2.271	2.242	2.252	0.42	-10.056
	1	Top-Ti	Ti-Li	2.806	2.773	2.794	-0.21	
			Ti-O		1.824	-	0.73	-3.051
			O-O		1.445	-	0.23	
$\text{TiC}\{100\}$	1	C-Ti	Ti-O	2.152	2.126	2.139	0.26	-3.506
			Ti-Li	2.532	2.531	2.532	-0.47	
			C-O	1.459	1.439	1.449	0.54	
	2	C-Ti	Ti-O	2.099	1.841	1.923	0.66	-3.696
			Ti-Li	2.984	2.748	2.913	-0.23	
			Ti-O	1.799	1.798	1.799	0.88	-2.316
	1	C-C	Ti-Li	2.966	2.758	2.889	-0.15	
			Ti-O		2.125	-	0.46	-1.375
			Ti-Li	2.927	2.848	2.895	-0.29	
	2	C-C	O-O	1.493	1.474	1.484	0.20	
			Ti-O		1.895	-	0.76	-0.636
			O-O	1.465	-	-	0.19	
$\text{TiC}\{100\}_{-\text{TiO}}$	1	C-Ti1	Ti-O	2.700	2.100	2.400	0.28	-1.809
			Ti-Li	2.239	2.722	2.730	-0.20	
			O-O		1.546	-	0.11	
	1	C-Ti2	Ti-O	1.762	1.724	1.762	0.93	-6.702
			Ti-Li	2.834	2.763	2.799	-0.16	
			Ti-O	1.767	1.762	1.764	0.92	-6.691
	1	B-Ti	Ti-Li	2.877	2.788	2.833	-0.15	
			Ti-O	1.809	1.793	1.801	0.98	-7.998
			Ti-Li	2.985	2.870	2.940	-0.11	
	1	Top-Ti	Ti-O		1.894	-	0.68	-1.407
			O-O	1.500	-	-	0.18	
			Ti-O	1.880	1.879	1.879	0.72	-1.356
	2	Top-Ti	O-O	1.488	1.448	1.448	0.20	

^aAdsorption energy, E_{ad} : eV/per Li_2O_2 cluster. ^bThese data are reproduced from our previous letter.³⁵

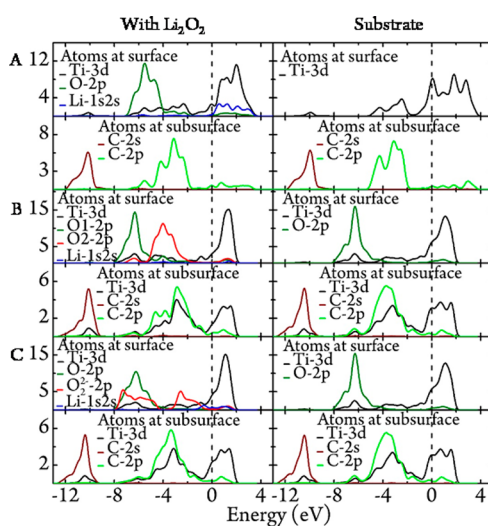


Figure 3. Angular momentum projected LDOS distribution for atoms at the interface and subinterface. (A) Two Li_2O_2 adsorption on the $\text{TiC}\{111\}_{-\text{Ti}}$ surface and planar Li_2O_2 in parallel with $\text{TiC}\{111\}$. (B) Two Li_2O_2 adsorption on the $\text{TiC}\{100\}_{-\text{TiO}}$ surface and planar Li_2O_2 in parallel with $\text{TiC}\{100\}$. (C) Two Li_2O_2 adsorption on the $\text{TiC}\{100\}_{-\text{TiO}}$ surface and planar Li_2O_2 perpendicular to the $\text{TiC}\{100\}$ surface.

properties of this layer have been described in Section 3.1. For the parallel adsorption configuration, we constructed three models: The first model, labeled as C-Ti1, had O-O in Li_2O_2 across over the center Ti atom in parallel with one of the diagonal Ti-O-Ti-O-Ti chains, while Li-Li was in parallel with the second diagonal Ti-O-Ti-O-Ti chain. Two diagonal chains share the center Ti atom and are perpendicular with each other. The second model (C-Ti2) is the same as the first except that the planar Li_2O_2 was rotated around the center Ti atom by 45° . The third model (B-Ti) used O-O as a bridge between the center Ti atom and an edge Ti atom, while two Li atoms are positioned above two O atoms in the surface TiO layer, respectively. After relaxation, the orientation of planar Li_2O_2 relative to the $\text{TiC}\{100\}_{-\text{TiO}}$ surface in the first model remained the same (Figure 2C1). Unlike the result from a similar model (Figure 2B1) for the adsorption on pristine $\text{TiC}\{100\}$, the planar structure of Li_2O_2 was kept intact with an O-O bond length reduced from 1.598 to 1.546 Å, and the distance between two Li atoms changed from 3.138 to 3.460 Å. The adsorption energy is -1.809 eV (C-Ti1 in Table 3), much smaller than -3.506 eV for the adsorption on the pristine $\text{TiC}\{100\}$ surface with the same initial Li_2O_2 orientation. The higher adsorption energy is because of destruction of O-O bonding and formation of not only Ti-O bonds but also C-O bonds (Figure 2B1). The relaxation of the second and the third models led to the same surface structure, a truncated square

pyramid (Figure 2C2) with two Ti atoms and two O atoms diagonally aligned at the four corners of the bottom and two Li atoms and two O atoms of Li_2O_2 at the four corners on the top. The Li atoms and the O atoms of the Li_2O_2 cluster are oriented above the O atoms and Ti atoms of the surface layer, respectively. Interestingly, though the O–O bond in Li_2O_2 was broken, the length changed from 1.598 to 2.830 Å, and four atoms still remained in the same original planar Li_2O_2 configuration. An adsorption energy of −6.691 eV (B–Ti in Table 3) was calculated, which is much larger than the value calculated for the first model. For the perpendicular adsorption configuration, there is only one potential model (Top-Ti), where Li_2O_2 hangs over the top of the Ti atom with the O–O bond perpendicular to the $\text{TiC}\{100\}\text{--TiO}$ surface (Figure 2C3). The adsorption energy calculated is −1.407 eV. The O–O bond length decreased from 1.598 to 1.500 Å, while the planar structure of Li_2O_2 was unchanged. When a second Li_2O_2 was added to both parallel and perpendicular models, we found that the adsorption energy increased from −6.702 to −7.998 eV per cluster for the parallel model and decreased slightly from −1.407 to −1.357 eV per cluster for the perpendicular adsorption. Atomic arrangement of Li and O atoms in the two Li_2O_2 cluster adsorption Top-Ti model (Figure 2C4) resembles $\text{O}_2\text{Li}_3\text{O}_4$ layers in the Li_2O_2 crystal structure, indicating a potential path for Li_2O_2 nucleation on the $\text{TiC}\{100\}\text{--TiO}$ surface.

For adsorption on the TiO-terminated $\text{TiC}\{100\}$ surface, Mulliken population analysis was also performed. Average bond length and overlap population for both parallel and perpendicular adsorption are listed in Table 3 as well. In comparison to the result of a similar analysis for the adsorption on the pristine $\text{TiC}\{100\}$ surface, a notable difference is that the overlap population of Ti–O bonding for two Li_2O_2 adsorption on the $\text{TiC}\{100\}\text{--TiO}$ surface (C–Ti2) is larger than that of Ti–O bonding for two Li_2O_2 on the pristine $\text{TiC}\{100\}$ surface (C–Ti), which explains why adsorption energy increased from −3.696 eV on the $\text{TiC}\{100\}$ surface to −7.998 eV on the $\text{TiC}\{100\}\text{--TiO}$ surface. For the perpendicular adsorption, two Li_2O_2 adsorption is unstable on the pristine $\text{TiC}\{100\}$ surface, while stable two Li_2O_2 adsorption can be formed on the $\text{TiC}\{100\}\text{--TiO}$ surface. Note that for perpendicular adsorption only one O atom from the Li_2O_2 cluster is bonded to the surface Ti. It can be also seen from Table 3 that, regardless of the surface orientations and the surface chemistry, the average overlap population of Ti–Li is all negative.

The angular momentum projected LDOS of the two Li_2O_2 parallel adsorption model of the $\text{TiC}\{100\}\text{--TiO}$ surface is plotted in Figure 3B in comparison to the similar adsorption on the surface of $\text{TiC}\{111\}\text{--Ti}$. Note that in both cases the original Li_2O_2 structure was destroyed, but the distribution of LDOS from adsorbed O atoms of Li_2O_2 is very much different. On the $\text{TiC}\{111\}\text{--Ti}$ surface, the DOS distribution is largely centered around −5.5 eV, which is close to the center of DOS distribution of −6.3 eV for O atoms in the TiO surface layer, suggesting that adsorption of Li_2O_2 on the $\text{TiC}\{111\}\text{--Ti}$ led to a surface oxidation, which is also noticeable from the LDOS distribution change of surface Ti-3d. However, on the $\text{TiC}\{100\}\text{--TiO}$ surface, the DOS distribution from adsorbed O atoms of Li_2O_2 is largely centered around −4.3 eV, clearly separated from the peak of the surface O atoms. Another noticeable difference is that the distribution of the Ti-3d DOS of the $\text{TiC}\{100\}\text{--TiO}$ surface remained largely the same before

and after adsorption, while a profound Ti-3d DOS distribution change resulted on the $\text{TiC}\{111\}\text{--Ti}$ surface after Li_2O_2 adsorption. The distribution of LDOS of two Li_2O_2 perpendicular adsorption on the $\text{TiC}\{100\}\text{--TiO}$ surface is plotted in Figure 3C. The DOS from O atoms of Li_2O_2 is largely distributed in two regions centered around −6.3 eV from O atoms bonded to the Ti atoms and around −2 eV from O atoms without direct bonding with Ti atoms. The O-2p states form Li_2O_2 , and O-2p states from the TiC surface and partial Ti-3d states are hybridized between −4 and −8 eV, responsible for surface adhesion.

3.3. Deposition of Li_2O_2 on the TiC surface. We treated TiC as the substrate and Li_2O_2 as the coating. The interface model was constructed by joining the TiC slab and Li_2O_2 slab together, then adding vacuum layers. To match between the TiC slab and Li_2O_2 slab, we considered the following four factors of (1) geometric match with low misfit factor η , (2) smooth surface with low surface energy, (3) surface conductivity, and (4) potential chemical bonding. Geometrically, we found that the $\text{Li}_2\text{O}_2\{1\bar{1}00\}$ surface has low misfit factor η of 3.75% (Figure S4 in Supporting Information) with the $\text{TiC}\{110\}$ surface, but the surface termination of $\text{Li}_2\text{O}_2\{1\bar{1}00\}$ with low surface energy (Table 1) is either too rough (O_2Li_3) or problematic ($\text{Li}_2\text{O}_2\text{Li}_3$ and $\text{Li}_1\text{O}_1\text{Li}_2\text{O}_2\text{Li}_3$) for interface bonding with the $\text{TiC}\{110\}$ surface. Our attempt to create $\text{Li}_2\text{O}_2\{1100\}/\text{TiC}\{110\}$ interface structures with either $\text{Li}_2\text{O}_2\text{Li}_3$ or $\text{Li}_1\text{O}_1\text{Li}_2\text{O}_2\text{Li}_3$ was unsuccessful, resulting in total destruction of the original atomic structure of Li_2O_2 .

Deposition on the $\text{TiC}\{111\}$ Surface. As described in our previous letter,³⁵ both $\text{TiC}\{111\}$ and $\text{Li}_2\text{O}_2\{0001\}$ surfaces are hexagonal with a relatively small misfit factor of 3.65%. For the $\text{Li}_2\text{O}_2\{0001\}$ surface, $\text{O}_2\text{Li}_3\text{O}_4$ termination of $\text{Li}_2\text{O}_2\{0001\}$ is conductive with the lowest surface energy. Therefore, we chose $\text{O}_2\text{Li}_3\text{O}_4$ termination to create the interface structure of $\text{Li}_2\text{O}_2\{0001\}/\text{TiC}\{111\}$. First, we tried to match $2 \times 2 \text{ O}_2\text{Li}_3\text{O}_4$ with the 2×2 Ti-terminated pristine $\text{TiC}\{111\}$ surface, in which each O atom at the bottom of $\text{O}_2\text{Li}_3\text{O}_4$ is directly placed on the top of a Ti atom of the $\text{TiC}\{111\}$ surface with potential to form strong Ti–O bonding. This construction was proved to be unstable. We were able to get the calculation for the first layer of $\text{O}_2\text{Li}_3\text{O}_4$ deposition to converge, but subsequent deposition was unsuccessful. In section 3.2, we found that when the two Li_2O_2 cluster adsorbed on the 2×2 Ti-terminated $\text{TiC}\{111\}$ surface, regardless of the initial Li_2O_2 cluster configurations (parallel or perpendicular), the surface relaxed to a saturated two-layer structure (Figure 2A3) in which four O atoms moved to hcp hollow. Each bonded to three Ti atoms of the TiC surface with an average bond length of 2.252 Å, while four Li atoms distributed to fcc hollows above O atoms. This configuration of Li and O atoms is the same as Li_1O_2 in the Li_2O_2 crystal structure (Figure S2 in Supporting Information), which can be viewed as the beginning of Li_2O_2 nucleation on the $\text{TiC}\{111\}\text{--Ti}$ surface. Furthermore, O atom arrangement in the O layer is the same as that in the top O layer of the oxidized $\text{TiC}\{111\}\text{--Ti}_\text{O}$ surface. These results led us to use $\text{TiC}\{111\}\text{--Ti}_\text{O}$ surface termination as the substrate and seek Li–O interface bonding and matched the $\text{TiC}\{111\}\text{--Ti}_\text{O}$ surface with a layer of $\text{O}_2\text{Li}_3\text{O}_3\text{Li}_1$ to create an interface model, denoted as 1 ML (one monolayer of $\text{O}_2\text{Li}_3\text{O}_3\text{Li}_1$, equivalent to a layer of Li_2O_2). By adding more layers of $\text{O}_2\text{Li}_3\text{O}_3\text{Li}_1$ sequentially, 2 ML and 3 ML were created and calculated. The results have been reported in our

previous letter.³⁵ A unit cell of Li_2O_2 structure was barely cut out from the 3 ML model to demonstrate bulk Li_2O_2 evolution as its thickness increased. To validate bulk-like Li_2O_2 formation, a 4 ML model was calculated. As shown in Figure 4A, the cut-

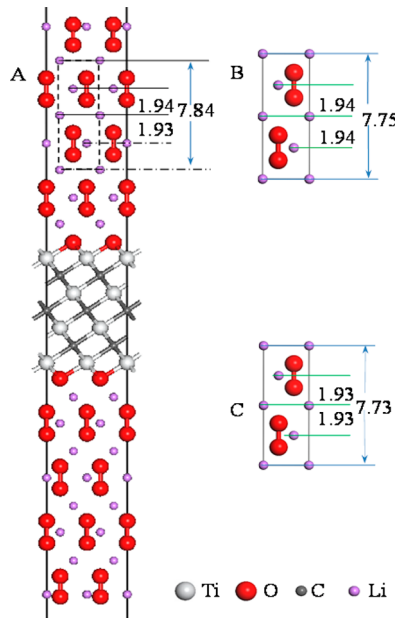


Figure 4. Comparison of (A) unit cell parameters calculated from Li_2O_2 coating on the $\text{TiC}\{111\}$ _ Ti_O surface to those calculated from (B) bulk Li_2O_2 and from (C) a standard unit cell of Li_2O_2 . (B) is reproduced from our published letter,³⁵ and C is reproduced with permission from refs 44 and 45.

out unit cell from the 4 ML model is closer to the calculated pure bulk Li_2O_2 cell (Figure 4B) and the standard unit cell of Li_2O_2 (Figure 4C).^{44,45} Similar to the 3 ML model, Li atoms near the surface are also moved up toward the surface relative to their position in the bulk, which might be partially responsible for the surface conductivity.

The conductive nature of Li_2O_2 coating is more clearly demonstrated from the LDOS of the 4 ML model (Figure 5). It can be seen that, due to contributions of Ti-3d and O-2p, the $\text{TiC}\{111\}$ _ Ti_O surface is conductive. From the first, through the second to third layer of $\text{O}_2\text{Li}_3\text{O}_4\text{Li}_1$, coatings are insulated

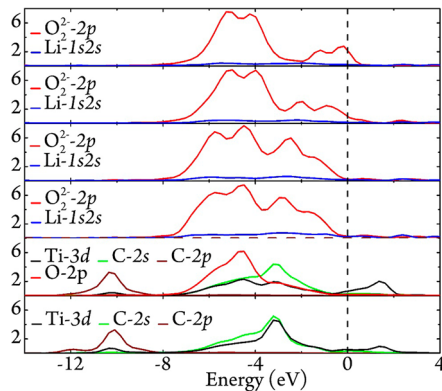


Figure 5. Angular momentum projected LDOS of the 4 ML model of the $\text{Li}_2\text{O}_2\{0001\}$ _ $\text{O}_2\text{Li}_3\text{O}_4/\text{TiC}\{111\}$ _ Ti_O interface. From the bottom to the top are TiC substrate, 1st, 2nd, 3rd, and 4th layer ($\text{O}_2\text{Li}_3\text{O}_4\text{Li}_1$) of the Li_2O_2 coating.

because the atomic structure of the coating grew into bulk Li_2O_2 alike (Figure 4A), and from the third through fourth layer to the surface, the coating is conducting. From Figure 5, an overlap of Li-2s states with O-2p states at the interface between -6 and -7 eV can be also seen, which is responsible for the interface adhesion.

Deposition on the $\text{TiC}\{100\}$ Surface. Finally, we evaluated the Li_2O_2 deposition on the $\text{TiC}\{100\}$ surface. The $\text{TiC}\{100\}$ surface is a dominated surface (100%) of TiC Wulff construction (Figure S1A in Supporting Information). In section 3.2, we have showed that the oxidized $\text{TiC}\{100\}$ surface ($\text{TiC}\{100\}$ _ TiO) is most stable for Li_2O_2 cluster adsorption, and the Li_2O_2 cluster perpendicular adsorption via direct Ti–O bonding is also stable. By following this lead, we constructed the $\text{Li}_2\text{O}_2\{0001\}/\text{TiC}\{100\}$ model using the oxidized $\text{TiC}\{100\}$ surface via Ti–O interface bonding. The $\text{TiC}\{100\}$ _ TiO surface lattice is square, and $\text{Li}_2\text{O}_2\{0001\}$ is hexagonal. To match the $\text{TiC}\{100\}$ _ TiO surface with the Li_2O_2 surface, we forced the hexagonal 2×2 $\text{Li}_2\text{O}_2\{0001\}$ layer of $\text{O}_2\text{Li}_3\text{O}_4$ into a square (from Figure 6A to 6B) and then

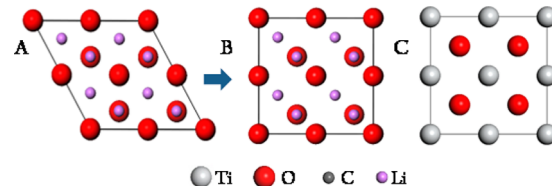


Figure 6. Schematic illustration of matching the 2×2 $\text{Li}_2\text{O}_2\{0001\}$ surface with the 2×2 $\text{TiC}\{100\}$ surface. Hexagonal Li_2O_2 surface (A) was forced to change into a square (B), then matched with the oxidized $\text{TiC}\{100\}$ _ TiO surface (C).

placed it on the top of the 2×2 $\text{TiC}\{100\}$ _ TiO surface (Figure 6C) to create a 1 ML model, in which each O atom at the bottom of this Li_2O_2 layer is positioned above a Ti atom on the $\text{TiC}\{100\}$ _ TiO surface. Similar to the case for the $\text{TiC}\{111\}$ surface, 2, 3, and 4 ML models were created by addition of the $\text{O}_2\text{Li}_3\text{O}_4\text{Li}_1$ layer sequentially.

Although significant strain should have been induced by forcing the hexagonal lattice of Li_2O_2 into a tetrahedral, it is surprising that all four models (1 ML–4 ML) converged to our preset cutoff value of 405 eV. The structural feature of four relaxed models is shown in Figure 7-1–7-4. The Li_2O_2 coating is bonded to the TiC substrate via Ti–O bonds, and the length of the Ti–O bond is in the range from 1.884 Å for the 1 ML model to 1.951 Å for the 4 ML model (Table S2), very close to the TiO band length of 1.91–2.04 Å in the TiO_2 oxides,⁵³ indicating a strong interface bonding. By comparing coating on the $\text{TiC}\{100\}$ _ TiO surface with that on the $\text{TiC}\{111\}$ _ Ti surface,³⁵ we noticed an interesting structural difference between two coatings. In the coating on the $\text{TiC}\{100\}$ _ TiO surface, the axis of O–O pairs is tilted relative to the *c*-direction, while in the coating on the $\text{TiC}\{111\}$ _ Ti surface, it orients in parallel with the *c*-direction. The axis of O–O pairs tilting on the $\text{TiC}\{100\}$ _ TiO surface can be explained by large strain induced when a hexagonal lattice of $\text{Li}_2\text{O}_2\{0001\}$ was forced into a tetragonal. The calculated angles of the O–O bond relative to the *c*-direction are between 11.4° and 22.3°. When coating thickness is increased, the O–O bond waggled back and forth. This happened because of the restriction placed on the atom movement of the model (limitation of software to handle straight up only model). In the case of a real deposition,

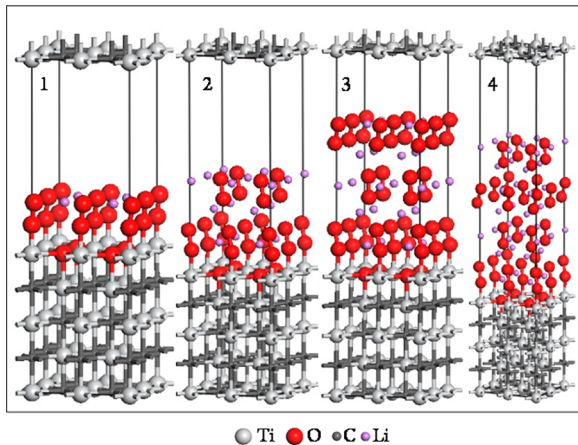


Figure 7. Relaxed interface models of $\text{Li}_2\text{O}_2\{0001\}$ – $\text{O}_2\text{Li}_3\text{O}_4$ with the oxidized $\text{TiC}\{100\}$ – TiO surface: (1) 1 ML, (2) 2 ML, (3) 3 ML, and (4) 4 ML.

the coating would grow most likely in one direction by following the direction of interface tilting. After the interface transition, the Li_2O_2 layer would gradually grow into its more stable hexagonal structure. **Figure 8** shows angular momentum

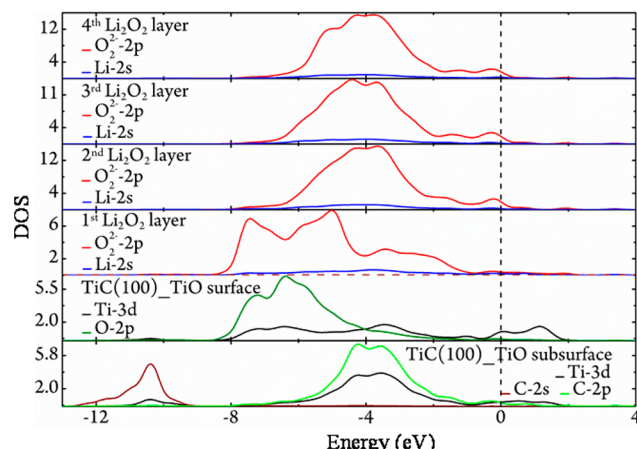


Figure 8. Angular momentum projected LDOS of the 4 ML model of the $\text{Li}_2\text{O}_2\{0001\}$ – $\text{O}_2\text{Li}_3\text{O}_4/\text{TiC}\{100\}$ – TiO interface. From the bottom to the top in order are oxidized $\text{TiC}\{100\}$ substrate, 1st, 2nd, 3rd, and 4th layer ($\text{O}_2\text{Li}_3\text{O}_4\text{Li}1$) of Li_2O_2 coating.

projected LDOS distribution from the $\text{TiC}\{100\}$ – TiO substrate, across the interface to the Li_2O_2 coating surface for the 4 ML model. It can be seen that at the interface there is a strong hybridization between Ti-3d and O-2p of the TiO surface layer and O-2p of the first Li_2O_2 layer. The DOS of O-2p from O atoms of the TiO layer and from the O-O pair of Li_2O_2 is largely overlapped around -6 eV, and small peaks around -3 eV are likely from the O atom of the O-O pair, which has no direct bonding with the Ti atom. Similar to the Li_2O_2 cluster adsorption on the surface of $\text{TiC}\{100\}$ – TiO discussed in a previous section (**Figure 3**), the hybridization of DOS of O-2p of the O-O pair and Ti-3d is responsible for the attractive surface bonding between two phases. The DOS of Ti-3d distributed above the Fermi level before Li_2O_2 coating was mostly moved below the Fermi level. The DOS at the Fermi level also decreased substantially, indicating a conductivity reduction. The DOS distribution for O-2p and Li-1s2s in the

second, third, and fourth layer ($\text{O}_2\text{Li}_3\text{O}_4\text{Li}1$) of the Li_2O_2 coating is essentially the same, centered largely around -4 eV with a small peak of O-2p located next to the Fermi level, resulting in a finite DOS at the Fermi level, so that the coating is conductive from the substrate to the surface. On the contrary, for the $\text{Li}_2\text{O}_2\{0001\}$ – $\text{O}_2\text{Li}_3\text{O}_4/\text{TiC}\{111\}$ – Ti_O interface model, the first and second layers of the coating are insulating because of their bulk-like Li_2O_2 lattice structure (**Figure 4**). Therefore, the conductivity in the interior of Li_2O_2 coating on the $\text{TiC}\{100\}$ – TiO surface is likely from strain on the lattice induced by the tetragonal restriction placed on the model during the relaxation.

Figure 9 plots the ideal work of adhesion W_{ad} dependence on the thickness of Li_2O_2 coating for the $\text{Li}_2\text{O}_2\{0001\}$ – $\text{O}_2\text{Li}_3\text{O}_4/$

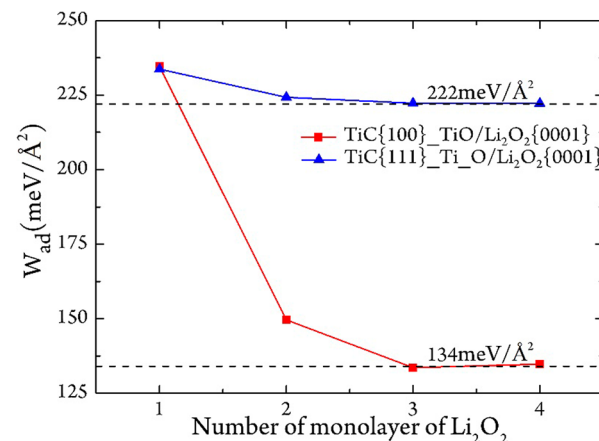


Figure 9. Ideal work of adhesion vs coating thickness of two interfaces. The data of 1st, 2nd, and 3rd layer adhesion on the $\text{TiC}\{111\}$ surface are reproduced from our previous letter.³⁵

$\text{TiC}\{100\}$ – TiO interface. For comparison, the same data from the $\text{Li}_2\text{O}_2\{0001\}$ – $\text{O}_2\text{Li}_3\text{O}_4/\text{TiC}\{111\}$ – Ti_O interface are also plotted. The adhesion strength for the first layer of Li_2O_2 deposition for both surfaces is almost the same. However, a bigger drop from 233 to 145 meV/ \AA^2 from the first layer to the second layer deposition was calculated for the coating on the $\text{TiC}\{100\}$ – TiO surface, likely due to the strain in the lattice. The relative small changes of adhesion strength on the $\text{TiC}\{111\}$ – Ti surface from the first layer to the second layer are consistent with the epitaxial growth nature of the Li_2O_2 coating. Adhesion strength plateaus of 134 and 222 meV/ \AA^2 are reached on the $\text{TiC}\{100\}$ – TiO and $\text{TiC}\{111\}$ surface, respectively.

The cross section total valence electron density distribution maps of 4 ML models of both $\text{Li}_2\text{O}_2\{0001\}$ – $\text{O}_2\text{Li}_3\text{O}_4/\text{TiC}\{111\}$ – Ti_O and $\text{Li}_2\text{O}_2\{0001\}$ – $\text{O}_2\text{Li}_3\text{O}_4/\text{TiC}\{100\}$ – TiO interfaces are depicted in **Figure 10A,B** together with their corresponding substrate. For the $\text{Li}_2\text{O}_2\{0001\}$ – $\text{O}_2\text{Li}_3\text{O}_4/\text{TiC}\{111\}$ – Ti_O interface, the cut plane is through Ti and C atoms along the long diagonal line of the 2×2 $\text{TiC}\{111\}$ surface lattice perpendicular to the $\text{TiC}\{111\}$ surface. For the $\text{Li}_2\text{O}_2\{0001\}$ – $\text{O}_2\text{Li}_3\text{O}_4/\text{TiC}\{100\}$ – TiO interface, the cut plane is through Ti and C/O atoms along one of the diagonal lines of the 2×2 $\text{TiC}\{100\}$ surface lattice perpendicular to the $\text{TiC}\{100\}$ surface. It can be seen that similar to the interior of Li_2O_2 the Li-O interface bonding is more ionic (**Figure 10A**, right) in comparison to the Ti-O interface bonding (**Figure 10B**, right). The electron density between Li and O atoms is

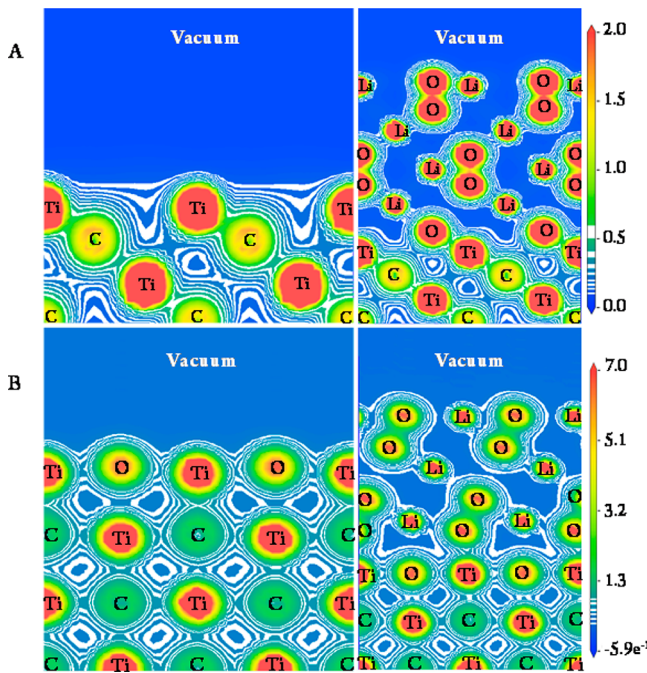


Figure 10. Total valence electron density map of (A) TiC{111} substrate (left), cut in the direction perpendicular to the {111} surface through Ti and C atoms along the long diagonal line of the 2×2 TiC{111} surface lattice, and the same cut with Li₂O₂ coating on the top (right), and (B) TiC{100}-TiO substrate (left), cut in the direction perpendicular to the {100} surface through Ti and O/C atoms along one of the diagonal lines of the 2×2 TiC{100} surface lattice, and the same cut with Li₂O₂ coating on the top (right).

higher in the interior of Li₂O₂ coating (Figure 10A, right) on the TiC{100}-TiO surface than that in the interior of Li₂O₂ coating on the TiC{111}-Ti_xO surface (Figure 10B, right), which is consistent with the observation that the interior of Li₂O₂ coating on the TiC{100}-TiO surface is conductive, while the interior of Li₂O₂ coating on the TiC{111}-Ti_xO surface is not.

4. SUMMARY AND CONCLUSION

With first-principles calculation based on the periodic density functional theory (DFT), we have investigated adhesion, structure, and electronic properties of Li₂O₂ clusters adsorbed on low index surfaces of TiC and the interface between Li₂O₂ and TiC as well as effects of oxidation of the TiC surface on these properties. Our results showed that oxidation increases the stability of TiC toward interaction with Li₂O₂ and facilitates deposition of Li₂O₂ on the TiC surface, which are in good agreement with experimental findings in the literature.¹⁸

First, we calculated bulk and surface properties of TiC and Li₂O₂ to identify the surface and surface terminations of both TiC and Li₂O₂ which are the most valuable for further investigation. The Wulff construction determined that the TiC{100} surface dominates surface termination of thermal equilibrium TiC crystallites at 100%. Hence, most of our calculation was performed on the TiC{100} and oxidized TiC{100} surfaces. Our calculation showed, in agreement with the literature,³⁴ the O₂Li₃O₄-terminated O-rich Li₂O₂{0001} surface is conductive and most stable; therefore, the termination was our choice for coating and interface model construction on the TiC surface. We approximated the oxidized TiC{100} surface by replacing C atoms with O atoms in the

surface layer of the TiC{100} surface and found that this simple exchange substantially increased the stability of the TiC{100} surface as evident by the surface energy reduction from 102 to 23 meV/Å².

Then, we studied planar Li₂O₂ cluster adsorption on the TiC surface in various configurations to probe the possibility of the nucleation of Li₂O₂ by introducing Li₂O₂ one by one on the TiC surface. We found that the stability of the TiC surface toward interaction with Li₂O₂ is related to the surface energy, from high to low in the sequence of TiC{100} > TiC{111}-Ti > TiC{110} > TiC{111}-C. The C-terminated TiC{111} surface is least stable, which was destroyed upon contact with the Li₂O₂ cluster. Oxidation of the TiC{100} surface further increases the stability of the TiC{100} surface toward interaction with Li₂O₂. Stable adsorptions of one and two Li₂O₂ both parallel and perpendicular to the TiC{100}-TiO surface were formed. Most importantly, for two Li₂O₂ adsorption in perpendicular configuration, two planar Li₂O₂ are bonded to the surface of TiC{100}-TiO in parallel to each other via two Ti-O bonds with the O-O axis perpendicular to the surface. This arrangement of Li and O atoms is similarly presented in the Li₂O₂ crystal structure, therefore suggesting the beginning of Li₂O₂ nucleation. On the 2×2 Ti-terminated TiC{111}-Ti surface, we found that, regardless of the initial placement of Li₂O₂ clusters, two Li₂O₂ cluster adsorption resulted in spontaneous destruction of planar Li₂O₂ clusters and formation of a saturated periodic surface structure with O atoms at the hcp hollow each bonded to three Ti atoms and Li atoms at the fcc hollow above the O layer. This atomic configuration is the same as Li₂O₂ (top two layers) in the Li₂O₂ crystal structure. Because the Ti-O bond length is similar to that in TiO₂, we considered that the Ti-terminated TiC{111} surface is oxidized. Therefore, periodic Li atoms on the top of the O layer were viewed as beginning deposition of the first atomic layer of Li₂O₂ on the TiC{111}-Ti_xO surface.

On the basis of studies of surface and Li₂O₂ adsorption above, we matched the low index Li₂O₂ surface of stable terminations with the low index TiC surface, Li₂O₂{1100}-Li₂O₂Li₃ and Li₂O₂{1100}-Li₁O₁Li₂O₂Li₃ with TiC{110}-Li₂O₂{0001}-O₂Li₃O₄ with TiC{111}-Ti and TiC{100}-TiO, to build interface models. We were unsuccessful to calculate convergent values for interface models of Li₂O₂{1100}-Li₂O₂Li₃/TiC{110} and Li₂O₂{1100}-Li₁O₁Li₂O₂Li₃/TiC{110} though both interfaces have a relatively small misfit factor η of 3.75%. Both Li₂O₂{0001}-O₂Li₃O₄ and TiC{111}-Ti_xO_x surfaces are hexagonal. A misfit factor η of 3.65% was calculated between them. We followed the lead obtained from adsorption study to create four interface models of 1, 2, 3, and 4 ML by adding the O₂Li₃O₄Li₁ layer (equivalent to a layer of Li₂O₂) sequentially on the TiC{111}-Ti_xO surface. The interface bonding is between Li and O atoms. We found that the models from 1 to 4 ML were all stable as if Li₂O₂ was grown epitaxially. A bulk-like lattice structure was obtained after the first Li₂O₂ layer of O₂Li₃O₄Li₁ deposition. Though the interior of the coating is insulated, an electron transfer path was maintained via surface conduction because the surface of O₂Li₃O₄ termination is conductive. Similarly, we constructed interface models of Li₂O₂{0001}-O₂Li₃O₄/TiC{100}-TiO by following the leads obtained from Li₂O₂ adsorption study. Instead of Li-O, we use Ti-O as the interface bonding. In spite of strain induced by forcing a hexagonal Li₂O₂ onto a square oxidized TiC{100} surface, stable interface models with Li₂O₂ coating from 1 to 4 ML were calculated. The LDOS

analysis showed strain-induced conductivity in the interior of the coating. The O–O bonds are tilted relative to the TiC surface at angles from 11.4° to 22.4° and waggle back and forth due to directional restriction of the model. The result suggests Li_2O_2 can be grown on the oxidized TiC{100} surface with a dihedral angle between 11.4° and 22.4°.

■ ASSOCIATED CONTENT

S Supporting Information

The Supporting Information is available free of charge on the ACS Publications website at DOI: [10.1021/acs.jpcc.5b06492](https://doi.org/10.1021/acs.jpcc.5b06492).

Cubic crystallographic structure of TiC, hexagonal crystallographic structure of Li_2O_2 , Wulff constructions of TiC and Li_2O_2 and planar structure of Li_2O_2 cluster; labeling scheme for unique atom layer in the Li_2O_2 structure; spin projected band structure of $\text{Li}_2\text{O}_2\{0001\}$ surface terminated with $\text{O}_2\text{Li}_3\text{O}_4$; 1×1 $\text{Li}_2\text{O}_2\{1\bar{1}00\}$ surface with terminations of $\text{Li}_2\text{O}_2\text{Li}_3$ and $\text{Li}_1\text{O}_1\text{Li}_2\text{O}_2\text{Li}_3$ matched with the 2×1 TiC{110} surface with a misfit factor of 3.75%, 2×2 $\text{Li}_2\text{O}_2\{0001\}$ surface matched with 2×2 Ti-terminated TiC{111} surface with a misfit factor 3.65%; surface energy of Li_2O_2 low index surface with different terminations and interplanar distance in the z direction for Li_2O_2 coating on the TiC{100}– TiO surface ([PDF](#))

■ AUTHOR INFORMATION

Corresponding Author

*E-mail: cniu@mail.xjtu.edu.cn. Phone: 02983395372.

Notes

The authors declare no competing financial interest.

■ ACKNOWLEDGMENTS

Financial support was provided by Xi'an Jiaotong University through a Grant for establishment of Center of Nanomaterials for Renewable Energy, and a CNSF grand 51221005.

■ REFERENCES

- (1) Abraham, K. M.; Jiang, Z. A Polymer Electrolyte-Based Rechargeable Lithium/Oxygen Battery. *J. Electrochem. Soc.* **1996**, *143*, 1–5.
- (2) Ogasawara, T.; Debart, A.; Holzapfel, M.; Novak, P.; Bruce, P. G. Rechargeable Li_2O_2 Electrode for Lithium Batteries. *J. Am. Chem. Soc.* **2006**, *128*, 1390–1393.
- (3) Poizot, P.; Laruelle, S.; Grangeon, S.; Dupont, L.; Tarascon, J. M. Nano-Sized Transition-Metaloxides as Negative-Electrode Materials for Lithium-Ion Batteries. *Nature* **2000**, *407*, 496–499.
- (4) Read, J.; Mutolo, K.; Ervin, M.; Behl, W.; Wolfenstine, J.; Driedger, A.; Foster, D. Oxygen Transport Properties of Organic Electrolytes and Performance of Lithium/Oxygen Battery. *J. Electrochem. Soc.* **2003**, *150*, A1351–A1356.
- (5) Debart, A.; Bao, J.; Armstrong, G.; Bruce, P. G. An O_2 Cathode for Rechargeable Lithium Batteries: The Effect of a Catalyst. *J. Power Sources* **2007**, *174*, 1177–1182.
- (6) Debart, A.; Paterson, A. J.; Bao, J.; Bruce, P. G. Alpha- MnO_2 Nanowires: A Catalyst for the O_2 Electrode in Rechargeable Lithium Batteries. *Angew. Chem., Int. Ed.* **2008**, *47*, 4521–4524.
- (7) Thapa, A. K.; Saimen, K.; Ishihara, T. Pd/ MnO_2 Air Electrode Catalyst for Rechargeable Lithium/Air Battery. *Electrochim. Solid-State Lett.* **2010**, *13*, A165–A167.
- (8) Thapa, A. K.; Ishihara, T. Mesoporous $\alpha\text{-MnO}_2/\text{Pd}$ Catalyst Air Electrode for Rechargeable Lithium–Air Battery. *J. Power Sources* **2011**, *196*, 7016–7020.
- (9) Lu, Y. C.; Gallant, B. M.; Kwabi, D. G.; Harding, J. R.; Mitchell, R. R.; Whittingham, M. S.; Shao-Horn, Y. Lithium-Oxygen Batteries: Bridging Mechanistic Understanding and Battery Performance. *Energy Environ. Sci.* **2013**, *6*, 750–768.
- (10) Thapa, A. K.; Shin, T. H.; Ida, S.; Sumanasekera, G. U.; Sunkara, M. K.; Ishihara, T. Gold-Palladium Nanoparticles Supported by Mesoporous Beta- MnO_2 Air Electrode for Rechargeable Li-Air Battery. *J. Power Sources* **2012**, *220*, 211–216.
- (11) Peng, Z. Q.; Freunberger, S. A.; Chen, Y. H.; Bruce, P. G. A Reversible and Higher-Rate $\text{Li}-\text{O}_2$ Battery. *Science* **2012**, *337*, 563–566.
- (12) Freunberger, S. A.; Chen, Y. H.; Drewett, N. E.; Hardwick, L. J.; Barde, F.; Bruce, P. G. The Lithium-Oxygen Battery with Ether-Based Electrolytes. *Angew. Chem., Int. Ed.* **2011**, *50*, 8609–8613.
- (13) Gallant, B. M.; Mitchell, R. R.; Kwabi, D. G.; Zhou, J. G.; Zuin, L.; Thompson, C. V.; Shao-Horn, Y. Chemical and Morphological Changes of $\text{Li}-\text{O}_2$ Battery Electrodes Upon Cycling. *J. Phys. Chem. C* **2012**, *116*, 20800–20805.
- (14) Lu, Y. C.; Kwabi, D. G.; Yao, K. P. C.; Harding, J. R.; Zhou, J.; Zuin, L.; Shao-Horn, Y. The Discharge Rate Capability of Rechargeable $\text{Li}-\text{O}_2$ Batteries. *Energy Environ. Sci.* **2011**, *4*, 2999–3007.
- (15) Freunberger, S. A.; Chen, Y. H.; Peng, Z. Q.; Griffin, J. M.; Hardwick, L. J.; Barde, F.; Novak, P.; Bruce, P. G. Reactions in the Rechargeable Lithium- O_2 Battery with Alkyl Carbonate Electrolytes. *J. Am. Chem. Soc.* **2011**, *133*, 8040–8047.
- (16) McCloskey, B. D.; Bethune, D. S.; Shelby, R. M.; Girishkumar, G.; Luntz, A. C. Solvents' Critical Role in Nonaqueous Lithium-Oxygen Battery Electrochemistry. *J. Phys. Chem. Lett.* **2011**, *2*, 1161–1166.
- (17) McCloskey, B. D.; Speidel, A.; Scheffler, R.; Miller, D. C.; Viswanathan, V.; Hummelshøj, J. S.; Norskov, J. K.; Luntz, A. C. Twin Problems of Interfacial Carbonate Formation in Nonaqueous $\text{Li}-\text{O}_2$ Batteries. *J. Phys. Chem. Lett.* **2012**, *3*, 997–1001.
- (18) Ottakam Thotiyil, M. M.; Freunberger, S. A.; Peng, Z. Q.; Chen, Y. H.; Liu, Z.; Bruce, P. G. A Stable Cathode for the Aprotic $\text{Li}-\text{O}_2$ Battery. *Nat. Mater.* **2013**, *12*, 1050–1056.
- (19) Ottakam Thotiyil, M. M.; Freunberger, S. A.; Peng, Z.; Bruce, P. G. The Carbon Electrode in Nonaqueous $\text{Li}-\text{O}_2$ Cells. *J. Am. Chem. Soc.* **2012**, *135*, 494–500.
- (20) McCloskey, B. D.; Scheffler, R.; Speidel, A.; Bethune, D. S.; Shelby, R. M.; Luntz, A. C. On the Efficacy of Electrocatalysis in Nonaqueous $\text{Li}-\text{O}_2$ Batteries. *J. Am. Chem. Soc.* **2011**, *133*, 18038–18041.
- (21) Gallant, B. M.; Kwabi, D. G.; Mitchell, R. R.; Zhou, J. G.; Thompson, C. V.; Shao-Horn, Y. Influence of Li_2O_2 Morphology on Oxygen Reduction and Evolution Kinetics in $\text{Li}-\text{O}_2$ Batteries. *Energy Environ. Sci.* **2013**, *6*, 2518–2528.
- (22) Renner, F. U.; Kageyama, H.; Siroma, Z.; Shikano, M.; Schoder, S.; Grunder, Y.; Sakata, O. Gold Model Anodes for Li-Ion Batteries: Single Crystalline Systems Studied by in Situ X-Ray Diffraction. *Electrochim. Acta* **2008**, *53*, 6064–6069.
- (23) Chen, J. Z.; Hummelshøj, J. S.; Thygesen, K. S.; Myrdal, J. S. G.; Norskov, J. K.; Vegge, T. The Role of Transition Metal Interfaces on the Electronic Transport in Lithium-Air Batteries. *Catal. Today* **2011**, *165*, 2–9.
- (24) Yang, Y.; Lu, H.; Yu, C.; Chen, J. M. First-Principles Calculations of Mechanical Properties of TiC and TiN. *J. Alloys Compd.* **2009**, *485*, 542–547.
- (25) Chen, K.; Kamran, S. Bonding Characteristics of TiC and TiN. *Model. Numer. Simul. Mater. Sci.* **2013**, *3*, 7–11.
- (26) Liu, L. M.; Wang, S. Q.; Ye, H. Q. Adhesion and Bonding of the Al/TiC Interface. *Surf. Sci.* **2004**, *550*, 46–56.
- (27) Arya, A.; Carter, E. A. Structure, Bonding, and Adhesion at the TiC(100)/Fe(110) Interface from First Principles. *J. Chem. Phys.* **2003**, *118*, 8982–8996.
- (28) Hwu, H. H.; Chen, J. G. G. Surface Chemistry of Transition Metal Carbides. *Chem. Rev.* **2005**, *105*, 185–212.

- (29) Johansson, L. I. Electronic and Structural-Properties of Transition-Metal Carbide and Nitride Surfaces. *Surf. Sci. Rep.* **1995**, *21*, 177–250.
- (30) Radin, M. D.; Tian, F.; Siegel, D. J. Electronic Structure of Li_2O_2 {0001} Surfaces. *J. Mater. Sci.* **2012**, *47*, 7564–7570.
- (31) Viswanathan, V.; Thygesen, K. S.; Hummelshøj, J. S.; Norskov, J. K.; Girishkumar, G.; McCloskey, B. D.; Luntz, A. C. Electrical Conductivity in Li_2O_2 and Its Role in Determining Capacity Limitations in Non-Aqueous $\text{Li}-\text{O}_2$ Batteries. *J. Chem. Phys.* **2011**, *135*, 214704.
- (32) Hummelshøj, J. S.; Blomqvist, J.; Datta, S.; Vegge, T.; Rossmeisl, J.; Thygesen, K. S.; Luntz, A. C.; Jacobsen, K. W.; Norskov, J. K. Communications: Elementary Oxygen Electrode Reactions in the Aprotic Li-Air Battery. *J. Chem. Phys.* **2010**, *132*, 071101.
- (33) Geng, W. T.; He, B. L.; Ohno, T. Grain Boundary Induced Conductivity in Li_2O_2 . *J. Phys. Chem. C* **2013**, *117*, 25222–25228.
- (34) Radin, M. D.; Rodriguez, J. F.; Tian, F.; Siegel, D. J. Lithium Peroxide Surfaces Are Metallic, While Lithium Oxide Surfaces Are Not. *J. Am. Chem. Soc.* **2012**, *134*, 1093–1103.
- (35) Wang, Z.; Sun, J.; Cheng, Y.; Niu, C. Adsorption and Deposition of Li_2O_2 on TiC{111} Surface. *J. Phys. Chem. Lett.* **2014**, *5*, 3919–3923.
- (36) Segall, M.; Lindan, P. J.; Probert, M.; Pickard, C.; Hasnip, P.; Clark, S.; Payne, M. First-Principles Simulation: Ideas, Illustrations and the Castep Code. *J. Phys.: Condens. Matter* **2002**, *14*, 2717.
- (37) Mattsson, A. E.; Schultz, P. A.; Desjarlais, M. P.; Mattsson, T. R.; Leung, K. Designing Meaningful Density Functional Theory Calculations in Materials Science-a Primer. *Modell. Simul. Mater. Sci. Eng.* **2005**, *13*, R1–R31.
- (38) Laasonen, K.; Pasquarello, A.; Car, R.; Lee, C.; Vanderbilt, D. Car-Parrinello Molecular-Dynamics with Vanderbilt Ultrasoft Pseudopotentials. *Phys. Rev. B: Condens. Matter Mater. Phys.* **1993**, *47*, 10142–10153.
- (39) Perdew, J. P.; Burke, K.; Ernzerhof, M. Generalized Gradient Approximation Made Simple. *Phys. Rev. Lett.* **1996**, *77*, 3865–3868.
- (40) Fischer, T. H.; Almlöf, J. General Methods for Geometry and Wave Function Optimization. *J. Phys. Chem.* **1992**, *96*, 9768–9774.
- (41) Monkhorst, H. J.; Pack, J. D. Special Points for Brillouin-Zone Integrations. *Phys. Rev. B* **1976**, *13*, 5188–5192.
- (42) Zhang, Y. F.; Vines, F.; Xu, Y. J.; Li, Y.; Li, J. Q.; Illas, F. Role of Kinetics in the Selective Surface Oxidations of Transition Metal Carbides. *J. Phys. Chem. B* **2006**, *110*, 15454–15458.
- (43) Fiorentini, V.; Methfessel, M. Extracting Convergent Surface Energies from Slab Calculations. *J. Phys.: Condens. Matter* **1996**, *8*, 6525–6529.
- (44) Föppl, H. Die Kristallstrukturen Der Alkaliperoxyde. *Z. Anorg. Allg. Chem.* **1957**, *291*, 12–50.
- (45) Cota, L. G.; de la Mora, P. On the Structure of Lithium Peroxide, Li_2O_2 . *Acta Crystallogr., Sect. B: Struct. Sci.* **2005**, *61*, 133–136.
- (46) Pearson, W. B.; Villars, P.; Calvert, L. D.; Metals, A. S. f. *Pearson's Handbook of Crystallographic Data for Intermetallic Phases*; American Society for Metals: Ohio, 1985.
- (47) Elliott, R. O.; Kempter, C. P. Thermal Expansion of Some Transition Metal Carbides. *J. Phys. Chem.* **1958**, *62*, 630–631.
- (48) Zhukov, V. P.; Gubanov, V. A.; Jepsen, O.; Christensen, N. E.; Andersen, O. K. Calculated Energy-Band Structures and Chemical Bonding in Titanium and Vanadium Carbides, Nitrides and Oxides. *J. Phys. Chem. Solids* **1988**, *49*, 841–849.
- (49) Chase, M. W., Jr. *NIST-JANAF Thermochemical Tables*; American Inst. of Physics: New York, 1998.
- (50) Xu, Y.; Shelton, W. A. O_2 Reduction by Lithium on Au(111) and Pt(111). *J. Chem. Phys.* **2010**, *133*, 024703.
- (51) Chan, M. K. Y.; Shirley, E. L.; Karan, N. K.; Balasubramanian, M.; Ren, Y.; Greeley, J. P.; Fister, T. T. Structure of Lithium Peroxide. *J. Phys. Chem. Lett.* **2011**, *2*, 2483–2486.
- (52) Shirotori, Y.; Sawada, K.; Ozawa, K.; Edamoto, K.; Otani, S. Photoelectron Spectroscopy Study of the Oxidation of TiC(100). *Japanese Journal of Applied Physics Part 1-Regular Papers Short Notes & Review Papers* **2003**, *42*, 1725–1731.
- (53) Park, J. Y.; Lee, C.; Jung, K. W.; Jung, D. Structure Related Photocatalytic Properties of TiO_2 . *Bull. Korean Chem. Soc.* **2009**, *30*, 402–404.
- (54) Mo, Y. F.; Ong, S. P.; Ceder, G. First-Principles Study of the Oxygen Evolution Reaction of Lithium Peroxide in the Lithium-Air Battery. *Phys. Rev. B: Condens. Matter Mater. Phys.* **2011**, *84*, 205446.
- (55) Seriani, N. Ab Initio Thermodynamics of Lithium Oxides: From Bulk Phases to Nanoparticles. *Nanotechnology* **2009**, *20*, 445703.
- (56) Lau, K. C.; Assary, R. S.; Redfern, P.; Greeley, J.; Curtiss, L. A. Electronic Structure of Lithium Peroxide Clusters and Relevance to Lithium-Air Batteries. *J. Phys. Chem. C* **2012**, *116*, 23890–23896.